



HAL
open science

Thermal core-mantle interaction: exploring regimes for 'locked' dynamo action

Ashley P. Willis, Binod Sreenivasan, David Gubbins

► **To cite this version:**

Ashley P. Willis, Binod Sreenivasan, David Gubbins. Thermal core-mantle interaction: exploring regimes for 'locked' dynamo action. *Physics of the Earth and Planetary Interiors*, 2007, 165 (1-2), pp.83. 10.1016/j.pepi.2007.08.002 . hal-00532125

HAL Id: hal-00532125

<https://hal.science/hal-00532125>

Submitted on 4 Nov 2010

HAL is a multi-disciplinary open access archive for the deposit and dissemination of scientific research documents, whether they are published or not. The documents may come from teaching and research institutions in France or abroad, or from public or private research centers.

L'archive ouverte pluridisciplinaire **HAL**, est destinée au dépôt et à la diffusion de documents scientifiques de niveau recherche, publiés ou non, émanant des établissements d'enseignement et de recherche français ou étrangers, des laboratoires publics ou privés.

Accepted Manuscript

Title: Thermal core-mantle interaction: exploring regimes for 'locked' dynamo action

Authors: Ashley P. Willis, Binod Sreenivasan, David Gubbins

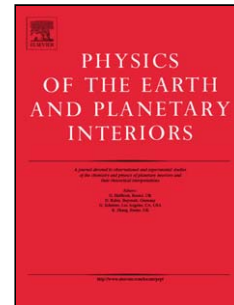
PII: S0031-9201(07)00163-X
DOI: doi:10.1016/j.pepi.2007.08.002
Reference: PEPI 4861

To appear in: *Physics of the Earth and Planetary Interiors*

Received date: 11-4-2007
Revised date: 27-7-2007
Accepted date: 12-8-2007

Please cite this article as: Willis, A.P., Sreenivasan, B., Gubbins, D., Thermal core-mantle interaction: exploring regimes for 'locked' dynamo action, *Physics of the Earth and Planetary Interiors* (2007), doi:10.1016/j.pepi.2007.08.002

This is a PDF file of an unedited manuscript that has been accepted for publication. As a service to our customers we are providing this early version of the manuscript. The manuscript will undergo copyediting, typesetting, and review of the resulting proof before it is published in its final form. Please note that during the production process errors may be discovered which could affect the content, and all legal disclaimers that apply to the journal pertain.



Thermal core-mantle interaction: exploring regimes for ‘locked’ dynamo action

Ashley P. Willis,

*Department of Mathematics, University of Bristol, University Walk, Bristol BS8
1TW, UK.*

Binod Sreenivasan & David Gubbins*

School of Earth and Environment, University of Leeds, Leeds LS2 9JT, UK.

Abstract

Possible effects on the geodynamo of lateral variations in heat flux from the core are explored, using two different patterns of heat flow from the core. One is based on lower mantle shear wave velocity and the other is the single spherical harmonic Y_2^2 . The self-consistent dynamo equations driven by thermal convection in a Boussinesq fluid are solved. Our choice of parameters is guided by earlier work on non-magnetic convection. We have already found a nearly steady solution locked to the tomographic boundary condition that bears a remarkable resemblance to the present day field; here we seek to understand this locked regime. Numerical considerations demand an artificially high Ekman number; we choose a low Rayleigh number and a Prandtl number of order unity. In this regime locking occurs when the underlying convection has an azimuthal wavelength similar to that of boundary conditions, as in the non-magnetic case. This is demonstrated where a drifting non-magnetic flow dominated by $m = 8$ rolls is converted to locked large scale-flow by the presence of a self-generated magnetic field. Large but geophysically reasonable variations in the

flux are required for locking. Dynamo action can fail at very large variation, where strong thermal winds disrupt the mechanism in this regime. If the Rayleigh number is too close to critical, the dynamo can fail for low variation, where the flow has a larger component driven by the boundary condition. Similarly, azimuthal flow at lower Prandtl numbers blurs the effect of the boundary condition.

1 Introduction

Hide (1967) was the first to suggest that the lower mantle influences the geomagnetic field through control of the dynamo. Since then several observations have been made that point to lower mantle effects: long-term changes in reversal frequency have been attributed to changes in the heat flux crossing the core-mantle boundary (CMB) (McFadden & Merrill, 1984); the large, high-latitude concentrations of flux (or “lobes”) that constitute the main dipole have been found to be relatively stable during the historical period (Bloxham & Gubbins, 1985) and there is a hint that they persist in the paleomagnetic time average (Gubbins & Kelly, 1993; Johnson & Constable, 1995); virtual geomagnetic poles (VGP) tend to follow a great circle passing through the same longitudes as the main lobes (Laj et al., 1991; Love, 1998); and weak secular variation in the Pacific (Fisk, 1931) (the so-called “Pacific dipole window”) may have persisted for much longer [(Doell & Cox, 1972), although the paleomagnetic evidence is disputed (Merrill & McElhinny, 1996)]. The great circle of stable flux concentrations corresponds roughly to the “ring-of-fire”

* Corresponding author.

Email addresses: a.willis@bristol.ac.uk (Ashley P. Willis),
binod@earth.leeds.ac.uk, gubbins@earth.leeds.ac.uk (Binod Sreenivasan & David Gubbins).

around the Pacific; it also encloses the Pacific dipole window.

This sparked speculation of a connection between the geodynamo and surface processes [e.g. Vogt (1975); Larson & Olson (1991)]. Seismic tomography has revealed a fast “doughnut” in the lowermost mantle beneath the ring-of-fire, no doubt associated with persistent subduction over many tens of millions of years. Cold regions in the lower mantle could cause preferential cooling of the core, downwelling, and concentration of radial magnetic flux at the core surface. This qualitative suggestion has now been explored in many convection and dynamo studies, mostly by imposing a heat flux or temperature boundary condition with the same geographic structure as a tomographic model of shear velocity (V_S) in the lowermost mantle [usually that of Masters et al. (1996)]. This assumes shear velocity is determined only by temperature and not by composition. The dominant pattern is a fast (cold) ring around the Pacific rim with slow (hot) regions beneath the Pacific and Africa - the sites of the superplumes. The largest term in a spherical harmonic expansion of the tomography is Y_2^2 , and many studies have simplified the boundary condition to this single harmonic, which carries the advantages of simplicity and symmetry.

The first numerical experiments considered non-magnetic convection with infinite Prandtl number (Pr) and temperature boundary conditions. They can be divided into studies of boundary-driven flow, or thermal winds, and convection driven from below modified by the boundary anomalies. Thermal winds do not involve downwelling beneath cold regions but pre-existing convection can: under the right circumstances convection becomes locked with downwelling limbs beneath cold boundary (Zhang & Gubbins, 1992, 1993b). At slightly supercritical Rayleigh number (R) the usual drifting pattern of “Busse” rolls becomes stationary, or “locked” to the boundary, provided the lateral variation

in boundary heating is sufficiently strong and the wavelength of convection with homogeneous boundary conditions is similar to the wavelength of the boundary anomalies.

Weakening the boundary heating leads, via a saddle-node bifurcation, to periodic solutions in which the pattern of cells drift at a non-uniform rate, slowing down when the downwelling limbs coincide with cold boundary and speeding up when they coincide with hot boundary. Analogous dynamics apply in a simple illustration of a submerged pendulum (Zhang & Gubbins, 1993a). The wavelength of the convection with homogeneous boundary conditions is largely determined by the Ekman number. Resonances were found when E was varied and RE held constant. Vigorous convection resulted when the two wavelengths were equal (resonance) or multiples of each other (secondary resonance) (Zhang & Gubbins, 1993b). In a subsequent study Zhang & Gubbins (1996) found boundary effects to be weaker at finite and low Pr .

Parallel work with heat flux boundary conditions (Gibbons & Gubbins, 2000; Gibbons et al., 2007) reinforced the importance of matching length scales between the boundary anomalies and the underlying convection. However, the response at moderate E is quite different because the dependence of the most unstable azimuthal wavenumber, m_c , or number of convection rolls at onset, is a much more complicated function of E than it is for temperature boundary conditions (see Gibbons et al. (2007)).

Addition of a magnetic field in subsequent models was less successful. Olson & Glatzmaier (1996) failed to find significant effects in magnetoconvection calculations even with very large lateral variations in heat flux. Nevertheless, Sarson et al. (1997) found nearly steady solutions in a 2.5D model with low degrees of freedom in azimuth (a mean mode, a sinusoid, and azimuthal shifts

of the sinusoid). Fully self-consistent geodynamo simulations with inhomogeneous thermal boundary conditions have been used to explore boundary effects on the frequency of reversals (Glatzmaier et al., 1999), the dominance of the dipole field in the past when lower mantle conditions were different (Bloxham, 2000a), the Pacific dipole window and secular variation (Bloxham, 2000b; Christensen & Olson, 2003), the time-average of the geomagnetic field (Olson & Christensen, 2002), preferred VGP reversal transition paths (Kutzner & Christensen, 2004), and more recently, time-averaged core surface flows (Aubert et al., 2007). These studies generally support the idea that lower mantle shear wave velocity correlates with some aspects of the time averaged field and statistical properties of the secular variation, but there is little evidence of simple locking or boundary resonance in these results, as was found in the non-magnetic experiments, nor is there any direct similarity between snapshots of the solutions and the present geomagnetic field. This requires the similarity between the present geomagnetic field and the time average to be a coincidence: we think this unlikely.

We therefore sought fully self-consistent dynamo solutions in which the magnetic field was locked to the boundary anomalies defined by tomography. Such a solution was found (Gubbins et al., 2007) in which the characteristic 4 main lobes persisted for many diffusion times *at the same sites as the main lobes of the geomagnetic field*. The correlation is striking, with dynamo and geomagnetic lobes within about 5° of each other. The parameters needed for this “locked” regime are geophysically improbable: we were forced to choose a large Roberts number $q = \kappa/\eta = 10$, where κ is the thermal diffusivity and η the electrical diffusivity. However, all geodynamo simulations suffer from unrealistic parameters as it is impossible to reach the correct E or R , and it is therefore not surprising that other parameter had to be changed in order to

obtain geophysically realistic effects.

The previous paper was driven by the observations, with the goal of finding a stationary or quasi-stationary solution that could be compared directly with the present geomagnetic field. The purpose of this paper is to explore the “locked dynamo” regimes further in order to understand the physical processes involved. The mathematical formulation of our model is described in the following section. Our initial exploration of the locked solution is described in Section 3. The regimes conducive and detrimental to locking are discussed in Section 4. The solution for the seismic shear wave velocity boundary condition is compared with the solution for the simplified Y_2^2 boundary condition. In the conclusions we highlight the principal accomplishments of this study.

2 Formulation

A Boussinesq fluid with finite electrical conductivity is modelled, confined between two concentric spherical surfaces that correspond to the Earth’s inner core boundary (ICB) and core-mantle boundary (CMB). The radius ratio is fixed at 0.35 corresponding closely to that of the Earth. Lengths are scaled by the thickness of the spherical shell d and time by d^2/κ , the thermal diffusion time, where κ is the thermal diffusivity, as we shall be primarily concerned with the effect of boundary heat flux variation on core convection. The magnetic field is scaled by $(2\Omega\rho\mu\eta)^{\frac{1}{2}}$ where Ω is the rate of rotation, ρ the density, μ the permeability of free space and η is the magnetic diffusivity. The non-dimensional equations are then

$$\frac{1}{Pr} (\partial_t + \mathbf{u} \cdot \nabla) \mathbf{u} - \nabla^2 \mathbf{u} = -\nabla \hat{p} + \frac{1}{qE} (\nabla \wedge \mathbf{B}) \wedge \mathbf{B}$$

$$+R\Theta\mathbf{r} - \frac{1}{E}\hat{\mathbf{z}} \wedge \mathbf{u}, \quad (1)$$

$$(\partial_t - \frac{1}{q}\nabla^2)\mathbf{B} = \nabla \wedge (\mathbf{u} \wedge \mathbf{B}), \quad (2)$$

$$(\partial_t - \nabla^2)\Theta = S - \mathbf{u} \cdot \nabla\Theta, \quad (3)$$

where

$$R = \frac{g\alpha\beta d^5}{\kappa\nu}, \quad E = \frac{\nu}{2\Omega d^2}, \quad Pr = \frac{\nu}{\kappa}, \quad q = \frac{\kappa}{\eta}, \quad (4)$$

are the Rayleigh, Ekman, Prandtl and Roberts numbers respectively. Written in this form, it is clear that the Rayleigh number measures the driving of the flow through the buoyancy force and that the Ekman number inversely measures rotational effects of the Coriolis force. Note that the prefactor $1/(qE)$ to the Lorentz term in (1) could be absorbed into the scaling for the magnetic field, and that the Roberts number, q , appears only in the magnetic diffusion term of (2). The role of the inertial term is inversely measured by the Prandtl number Pr , but also depends on the magnitude of the flow. Non-magnetic convection is governed only by the parameters R , E and Pr . For no flow, $\mathbf{u} = \mathbf{0}$, a uniform internal (dimensional) heat source S' leads to the temperature profile

$$\hat{\Theta} = \frac{\beta}{2}(r_0^2 - r^2), \quad \beta = \frac{1}{3\kappa} S'. \quad (5)$$

The temperature in (3) has been scaled by βd^2 giving the dimensionless volumetric heat source $S = 3$. No-slip boundary conditions are imposed on the flow. The inner core is fixed at a uniform temperature, is not free to rotate, and is electrically conducting. The outer boundary is electrically insulating with an imposed, laterally varying heat flux. Two patterns of laterally varying boundary condition are used, one the single spherical harmonic Y_2^2 and the other a ‘‘tomographic’’ boundary condition based on the shear wave velocity

at the base of the mantle (Masters et al., 1996). The degree of lateral variation in heat flux is measured by a horizontal Rayleigh number, R_H , based on the maximum lateral variation of heat flux at the outer boundary. The ratio, ϵ , is therefore

$$\epsilon = \frac{\text{maximum flux variation}}{\text{mean flux}} = \frac{R_H}{R}, \quad (6)$$

which is $\epsilon = 0$ for the homogeneous condition. For the tomographic boundary condition an $\epsilon = 1$ corresponds to peaks of -55% to $+45\%$ of the mean radial heat flux; for the Y_2^2 mode it corresponds to $\pm 50\%$. The tomographic boundary condition is plotted in Figure 1.

Velocity and magnetic fields are expressed in terms of toroidal and poloidal potentials,

$$\mathbf{B} = \nabla \wedge (\mathcal{T}\mathbf{r}) + \nabla \wedge \nabla \wedge (\mathcal{P}\mathbf{r}), \quad \mathbf{u} = \nabla \wedge (T\mathbf{r}) + \nabla \wedge \nabla \wedge (P\mathbf{r}) \quad (7)$$

These potentials are expanded in terms of spherical harmonics in the form,

$$A(\theta, \phi) = \sum_{l=0}^{\infty} \sum_{|m| \leq l} A_{lm} \hat{Y}_l^m(\theta, \phi), \quad \text{where, } \hat{Y}_l^m(\theta, \phi) = P_l^{|m|}(\cos \theta) e^{im\phi}, \quad (8)$$

where the P_l^m are the associated Legendre functions. The spherical harmonics are normalised such that

$$\int_0^{2\pi} \int_0^{\pi} (\hat{Y}_l^m)^2 \sin \theta \, d\theta \, d\phi = 2\pi \frac{2(2 - \delta_{m0})}{2l + 1}. \quad (9)$$

Taking the r -component of the induction equation (2) and the r -component of its curl leads to two second-order equations, one for each of the potentials,

$$\left(\partial_t - \frac{1}{q} \nabla^2\right) \mathcal{P} = \frac{r}{l(l+1)} \hat{\mathbf{r}} \cdot \mathbf{N}, \quad (10)$$

$$(\partial_t - \frac{1}{q}\nabla^2)\mathcal{T} = \frac{r}{l(l+1)} \hat{\mathbf{r}} \cdot \nabla \wedge \mathbf{N}. \quad (11)$$

where \mathbf{N} represents the nonlinear terms on the right hand sides of each equation. The equations also separate for each of the spherical harmonic modes. Indices l, m on the potentials in (10) and (11) have been dropped. A property of spherical harmonics gives $\nabla^2 \equiv \partial_{rr} + 2r^{-1}\partial_r - l(l+1)r^{-2}$. Division by l on the right hand side is safe as $\nabla \cdot \mathbf{B} = 0$ implies no $l = 0$ harmonic is required. Nonlinear terms, \mathbf{N} , are evaluated in real space and then transformed back to spectral coefficients. To avoid aliasing of higher wavenumbers introduced by the nonlinear terms, they are evaluated on extra points according to the ‘three-halves’ rule (Orszag, 1971). The boundary conditions are $\mathcal{T} = 0$ and $(\partial_r + (l+1)r^{-1})\mathcal{P} = 0$ on the outer insulating boundary; potentials and their first derivatives are continuous across the boundary to the conducting inner core.

Taking the r -components of the curl and curl-curl of the momentum equation, one may write three second-order equations,

$$(\frac{1}{Pr}\partial_t - \nabla^2)T = \frac{r}{l(l+1)} \hat{\mathbf{r}} \cdot \nabla \wedge \mathbf{N}, \quad (12)$$

$$(\frac{1}{Pr}\partial_t - \nabla^2)P = g \quad (13)$$

$$-\nabla^2 g = \frac{r}{l(l+1)} \hat{\mathbf{r}} \cdot \nabla \wedge \nabla \wedge \mathbf{N}. \quad (14)$$

with no slip boundary conditions $T = 0$, $P = 0$, $\partial_r P = 0$. Although there are four boundary conditions on the P and none on g , any difficulty is easily by-passed using the influence-matrix method, Peyret (2002). They are satisfied to numerical precision at little additional expense. Our method is similar to that of Tilgner (1999). However, rather than another spectral expansion in radius a seven-point finite difference stencil is used to conserve memory

requirements, improve computation time, and ease parallelisation. The radial mesh points are located at zeros of the appropriate order Chebyshev polynomial and are clustered near the boundaries. The solution to system (13) and (14) is expressed as a linear combination of the solutions to three independent systems, $P = \bar{P} + a P_G + b P'_G$, where

$$\begin{cases} \mathcal{X}\bar{P} = \bar{g}, \\ \mathcal{Q}\bar{g} = f, \end{cases} \quad \begin{cases} \mathcal{X}P_G = g_G, \\ \mathcal{Q}g_G = 0, \end{cases} \quad \begin{cases} \mathcal{X}P'_G = g'_G, \\ \mathcal{Q}g'_G = 0, \end{cases} \quad (15)$$

with conditions, $g_G = 1$, $g'_G = 0$ on the inner boundary, $g_G = 0$, $g'_G = 1$ on the outer boundary, and $\partial_r \bar{P} = \partial_r P_G = \partial_r P'_G = \bar{g} = 0$ on both. \mathcal{X} and \mathcal{Q} represent the operators on the left-hand sides of (13) and (14). The system for \bar{P} is solved at each timestep, where f is the time-dependent right-hand side of (14). The solutions for P_G and P'_G are independent of time and may be precomputed. The solution for P satisfying all boundary conditions is the superposition $P = \bar{P} + a P_G + b P'_G$, where the coefficients a, b are determined by the no-penetration condition, $P = 0$. They are found by solving the influence matrix equation

$$\begin{bmatrix} P_G(r_i) & P'_G(r_i) \\ P_G(r_o) & P'_G(r_o) \end{bmatrix} \begin{bmatrix} a \\ b \end{bmatrix} = - \begin{bmatrix} \bar{P}(r_i) \\ \bar{P}(r_o) \end{bmatrix}. \quad (16)$$

The temperature is also expanded in spherical harmonics and the temperature equation solved in similar fashion to the induction and momentum equations, using the same finite difference schemes and evaluating the nonlinear advective term by the transform method. In the following calculations 55 radial points were used and, as the Rayleigh number was small, harmonics up to $l = 36$

were found to be sufficient. Spectra for the magnetic and velocity fields fell by approximately 3 orders of magnitude by the truncation point. The locked dynamo for the tomographic boundary condition (following section) was also checked for l up to 48, for which no differences were identifiable. The timestep size was controlled using information from a predictor-corrector method where the error showed second-order convergence. The code shows excellent agreement with the dynamo benchmark (Christensen et al., 2001) and other recent dynamo calculations (Olson et al., 1999).

3 Parameter selection: tomographic boundary condition

Under strong rotation, the Ekman number E is small and the primary force balance is between the magnetic, Archimedean (buoyancy) and Coriolis forces represented on the right-hand side of equation (1), the so-called MAC or magnetogeostrophic balance. This is not the complete story, however, as the Coriolis force does not affect components of the flow that are dependent only on the cylindrical radius from the axis. Strong zonal flows can occur if the inertial term becomes significantly large, which happens when Pr is low (Simitev & Busse, 2003; Sreenivasan & Jones, 2006). At smaller E and larger Pr the magnetogeostrophic, or geostrophic balance in the non-magnetic case, is established, which has the effect of pushing the resulting flow patterns onto smaller length scales, much smaller than are likely to be of significance in magnetic field generation. It is thought, however, that the presence of a strong magnetic field may cause the flow to evolve on larger length scales. It has been suggested that, if the field became sufficiently weak, the flow may begin to evolve on smaller length scales and that the magnetic field may die altogether (Zhang & Gubbins, 2000). For the moment, we wish to ensure that the correct

balance of terms is achieved.

We are guided by the linear stability results of non-magnetic rotating convection with homogeneous heat flux boundary conditions. Figure 6 of Gibbons et al. (2007) gives the mode with most unstable azimuthal wavenumber, m_c , as a function of Ekman and Prandtl numbers and $r_i/r_o = 0.4$. Here the critical Rayleigh number, R_c , has been recalculated at $r_i/r_o = 0.35$ but the critical m_c appear to be essentially identical. For fixed moderate Pr there is a sharp transition from $m_c = 1$ to m_c of order 10 as E is decreased. This is quite different from the case of fixed temperature boundary conditions, where the increase of m_c smoothly asymptotes to $E^{-1/3}$ as $E \rightarrow 0$. At low E the difference in behaviour between temperature and heat flux boundary conditions disappears, and the $E^{-1/3}$ law is followed in both cases, but this regime is numerically difficult in the non-magnetic case and impractical for dynamo calculations. We therefore chose E to be smaller than where the jump in m_c occurs, at around 2×10^{-4} for moderate Pr . Initially we chose $Pr = 1$ and $E = 1.2 \times 10^{-4}$, for which the onset of thermal convection occurs at $R_c E = 23.3$ and $m_c = 8$. Nonlinear calculations with non-magnetic convection showed that our flow remained of similar scale provided R was not highly supercritical, progressing from quasi-periodic rolls to rolls plus an increasing number of chaotic defects as R/R_c is increased.

Small magnetic fields were added to each of the non-magnetic flows with homogeneous boundary conditions to test for kinematic dynamo action, but none was found for values of q up to 100. A dynamo was found at $q = 10$ by adding an initial dipolar field large enough for the nonlinear feedback through the Lorentz force to be significant: compare left-hand plots (for homogeneous boundary conditions) in Figure 2. Both dynamo and non-magnetic flows are

highly chaotic, the dynamo much more so, but with longer length-scales. Lowering q to 8, the dynamo decayed and the flow reverted to that of non-magnetic convection.

The next step was to explore the effect of the inhomogeneous tomographic boundary condition on the dynamo solution, increasing the boundary inhomogeneity until a significant thermal coupling was seen. Dynamo solutions at all values of ϵ generated magnetic fields with flux patches in high latitudes, at least for short intervals of time. At $\epsilon = 0.3$ only a slight preference in longitude was observed in these patches; for 0.6 the high-latitude patches would often stay close to the cold regions, but sometimes drifted away or split in two; see Figure 3. When ϵ was increased further to 0.9, the field was strongly locked although not completely stationary — the magnetic flux lobes are subject to small east-west motions, but of no more than a few degrees — so that snapshots are representative of the field configuration at any time.

In addition to the flows for homogeneous boundary conditions compared in Figure 2 are the non-magnetic and dynamo solutions for the tomographic boundary condition (right-hand plots). Flow is weak below the hot regions (where the boundary heat flux is low) for both dynamo and non-magnetic flows. The non-magnetic flow is more chaotic than the dynamo flow, however, and is smaller scale. The lesser influence of the boundary condition on the non-magnetic flow may be attributed to a disparity of length scales — the rolls being much smaller than the dominant $m = 2$ scale in the boundary condition. In the dynamo, downwellings fix to the boundary condition, the rolls are larger where the field is stronger. Beneath the cool regions upwellings are broader and the return flow relatively quiescent. The dominant high-latitude flux patches occur as a direct result of the downwellings (Olson et al., 1999).

They are convincingly correlated with those in the observations [see Figure 3 and the discussion in Gubbins et al. (2007)]. Rolls of smaller scale are occasionally shed [for example the patch at approximately 70° E in Figure 2(d)] and correspond to quickly moving equatorial flux patches, of either polarity, moving predominantly westwards. They occur more frequently in the model with $\epsilon = 0.6$ where the locking is not as strong (Figure 3). Whether they are related to similar features in the Earth's field is unclear at this stage.

4 Regimes for locked dynamo action: the Y_2^2 boundary condition

The tomographic boundary condition is a complicated function involving many spherical harmonic terms, and perhaps more significantly many azimuthal wavenumbers. The largest spherical harmonic coefficient is for Y_2^2 , reflecting the rather symmetrical pattern of a cold ring beneath the Pacific rim and hot regions beneath the central Pacific and Africa. We therefore imposed a Y_2^2 pattern of heat flux, with maxima at $\phi = 0, \pi$ and minima at $\phi = \pm\pi/2$.

We consider runs with the Y_2^2 boundary condition and initially $Pr = 1$, $\epsilon = 1.0$. At $E = 10^{-4}$ and $q = 10$ locking is observed when $R/R_c = 1.43$; at $E = 5 \times 10^{-5}$ locking is observed for $q = 15$ and $R/R_c = 1.13$. As seen in Table 1, the dynamo at $E = 5 \times 10^{-5}$ has a larger magnetic Reynolds number, R_m , which is the most likely explanation for the larger volume-averaged magnetic field, reflected in the value of the Elsasser number, Λ (≈ 4).

The convection pattern for $E = 10^{-4}$, $\epsilon = 1$ is shown in Figure 4(b). The convection is organized into two dominant downwellings slightly to the east of the longitudes of maximum heat flux. These downwellings draw down toroidal magnetic field lines producing radial components close the equatorial plane,

see Figures 4(c,d) and 5. As B_ϕ changes sign across the equator so the resulting patches are of opposing sign. Similar features are seen frequently in kinematic studies above downwellings (Gubbins et al., 2000).

Increasing ϵ to values much greater than 1.5 produces thermal gradients that upset the $m = 2$ convection pattern, again leading to failure of the dynamo. A similar effect has been observed by Olson & Christensen (2002), who found with both Y_2^2 and Y_2^0 heat flow patterns that dynamo action could not be sustained when the amplitude of the heat flow heterogeneity exceeded the average boundary heat flow. When ϵ is lowered to 0.6 or below, keeping all other parameters the same, the dynamo fails leaving the nonmagnetic convective pattern shown in Figure 4(a). This result is significant because it implies that in the low-Rayleigh number regime dynamo action can be sustained in the locked state by a large enough lateral variation at the boundary. Note that this failure of dynamo action at smaller ϵ did not occur for the tomographic boundary condition, but there E was slightly higher. Nevertheless, this surprising result may point to the indirect role played by harmonics other than Y_2^2 in producing dynamo action; the effect of individual components of the tomographic boundary condition on the dynamo solution is an ongoing study. On the other hand, with the smaller R/R_c for this case, it is likely that the boundary inhomogeneity plays an increased part in driving the flow.

To isolate the effect of inertia on locking we consider the case where $\epsilon = 1$, $RE = 30$ and $q = 15$ are fixed and only Pr is varied. If Pr is sufficiently large the dynamos operate in an asymptotic regime where the solutions are nearly identical. Raising Pr from 1 to 2 changes R/R_c from 1.13 to 0.84 for non-magnetic flow, but the dynamo flows are indistinguishable. Both the magnetic Reynolds number, $R_m \approx 230$ and the Elsasser number, $\Lambda \approx 4$ are almost un-

changed (see Table 1). This suggests that the dynamo is in magnetogeostrophic balance. The slightest introduction of inertia, however, is sufficient to disturb the geostrophy of the downwellings that concentrate the poloidal field at high latitudes (Olson et al., 1999; Sreenivasan & Jones, 2006). Reducing Pr to 0.67 causes failure of dynamo action. This result highlights the sensitivity of the dynamo and the important role the downwellings play in the dynamo cycle. In these regions toroidal field is converted to poloidal field, see Olson et al. (1999), although this is often not clearly observed in dynamo calculations with highly supercritical Rayleigh numbers and homogeneous boundaries.

5 Conclusions

Realistic geophysical parameters are low E , high R , and assuming turbulence acts to equalise the diffusivities, Prandtl numbers of order 1. The value of the lateral heat flux parameter ϵ is not known, but is chosen to be order 1 in many models, Aubert et al. (2007) suggest a value of 0.3. It is not possible to reach realistic values for all these parameters in one model, however, two independent arguments based on estimates of heat flux from the core (Jones, 2000; Gubbins, 2001) point to an R not as high as was once feared. Low- E , weakly-diffusive dynamo regimes are explored on the supposition that they will be a better representation of convection in the Earth's core, but we must ensure that they produce magnetic fields that satisfy observational constraints. It is also important to identify the conditions under which boundary inhomogeneities control core convection.

In this study we presented dynamo regimes that nearly lock core convection and the magnetic field to prescribed boundary inhomogeneities. We did this in

order to understand the locking process rather than to simulate the geodynamo directly, but the observations strongly suggest that this regime is relevant for the geodynamo. A moderate E was essential to simplify the calculations and allow exploration of a large volume of parameter space. Beyond that, our choices of E were made to produce convection with azimuthal wavelengths comparable with those of the imposed boundary conditions. Low R is the obvious choice when searching for nearly-steady solutions. At moderate to large Pr for this case the dynamo is in magnetogeostrophic balance. This leaves only q , which for negligible inertia appears only in the magnetic diffusion term, and thus must be high enough to allow dynamo action (high q follows from low magnetic diffusivity, and therefore controls the magnetic Reynolds number). These considerations determined the choice of parameters for the locked solution in Gubbins et al. (2007).

Parameter choices are limited by the twin requirement of dynamo action and locking to the boundary. We find the following general results:

- (1) Increasing the lateral heating parameter ϵ much beyond 1 leads to dynamo failure, frustrating our quest for a locked solution [also see Olson & Christensen (2002)]. If R/R_c is too low, then for a boundary driven flow the dynamo can fail for ϵ too small.
- (2) Lowering E makes locking more difficult. A probable reason for this is an observed reduction in length scale of the convection, as is expected from asymptotic results for rapidly rotating convection at marginal stability, giving a disparity of scales with the boundary anomalies. Lowering E may also raise R/R_c ...
- (3) Raising R/R_c to moderately high values (~ 4) here causes the dynamo to fail, possibly due to a progression to smaller scales or by the introduction

of inertia. In this harder-driven regime it is likely that a further increase of R/R_c will again produce dynamo action where, although the fluid motion is largely decoupled from the boundary inhomogeneity, effects may be seen in the time average (Olson & Christensen, 2002; Aubert et al., 2007). Dynamo scenarios which counter the negative affect on locking, encountered by an increase in R/R_c or a decrease in E , are the subject of further study Sreenivasan & Gubbins (2007).

- (4) Low Pr is also detrimental to locking and dynamo action. This regime exhibits a rapid azimuthal flow which blurs the lateral boundary variations.

Acknowledgement

This work was supported by NERC consortium grant *Deep Earth Systems* O/2001/00668. The authors thank the referees for many useful suggestions.

References

- Aubert, J., Amit, H., & Hulot, G., 2007. Detecting thermal boundary control in surface flows from numerical dynamos, *Phys. Earth Planet. Int.*, **160**, 143–156.
- Bloxham, J., 2000. Sensitivity of the geomagnetic axial dipole to thermal core-mantle interactions, *Nature*, **405**, 63–65.
- Bloxham, J., 2000. The effect of thermal core-mantle interactions on the paleomagnetic secular variation, *Philos. Trans. R. Soc. London Ser. A*, **358**, 1171–1179.
- Bloxham, J. & Gubbins, D., 1985. The secular variation of the Earth's magnetic field, *Nature*, **317**, 777–781.
- Christensen, U., Aubert, J., Cardin, P., Dormy, E., Gibbons, S., Glatzmaier, G. A., Grote, E., Honkura, Y., Jones, C., Kono, M., Matsushima, M., Sakuraba, A., Takahashi, F., Tilgner, A., Wicht, J., & Zhang, K., 2001. A numerical dynamo benchmark, *Phys. Earth Planet. Int.*, **128**, 25–34.
- Christensen, U. R. & Olson, P., 2003. Secular variation in numerical geodynamo models with lateral variations of boundary heat flow, *Phys. Earth Planet. Int.*, **138**, 39–54.
- Doell, R. R. & Cox, A. V., 1972. The Pacific geomagnetic secular variation anomaly and the question of lateral uniformity in the lower mantle, in *The nature of the solid earth*, edited by E. C. Robertson, pp. 245–284, McGraw-Hill, New York, NY.
- Fisk, H. W., 1931. Isopors and isoporic movement, *Bull. Int. Geodet. Geophys. Union*, **8**, 280–292.
- Gibbons, S. & Gubbins, D., 2000. Convection in the Earth's core driven by lateral variations in the core-mantle boundary heat flux, *Geophys. J. Int.*, **142**, 631–642.

- Gibbons, S. J., Gubbins, D., & Zhang, K., 2007. Convection in a rotating spherical fluid shells with inhomogeneous heat flux at the outer boundary, *Geophys. Astrophys. Fluid Dyn.*, **in press**.
- Glatzmaier, G. A., Coe, R. S., Hongre, L., & Roberts, P. H., 1999. The role of the Earth's mantle in controlling the frequency of geomagnetic reversals, *Nature*, **401**, 885–890.
- Gubbins, D., 2001. The Rayleigh number for convection in the Earth's core., *Phys. Earth Planet. Int.*, **128**, 3–12.
- Gubbins, D. & Kelly, P., 1993. Persistent patterns in the geomagnetic field during the last 2.5 Myr, *Nature*, **365**, 829–832.
- Gubbins, D., Barber, C. N., Gibbons, S., & Love, J. J., 2000. Kinematic dynamo action in a sphere: II symmetry selection, *Proc. R. Soc.*, **456**, 1669–1683.
- Gubbins, D., Willis, A. P., & Sreenivasan, B., 2007. Correlation of earth's magnetic field with lower mantle thermal and seismic structure, *Phys. Earth Planet. Int.*, **162**, 256–260.
- Hide, R., 1967. Motions of the Earth's core and mantle, and variations of the main geomagnetic field, *Science*, **157**, 55–56.
- Johnson, C. & Constable, C., 1995. The time-averaged geomagnetic field as recorded by lava flows over the past 5 Myr, *Geophys. J. Int.*, **122**, 489–519.
- Jones, C. A., 2000. Convection-driven geodynamo models, *Proc. R. Soc.*, **358**, 873–897.
- Kutzner, C. & Christensen, U. R., 2004. Simulated geomagnetic reversals and preferred virtual geomagnetic pole paths, *Geophys. J. Int.*, **157**, 1105–1118.
- Laj, C. A., Mazaud, A., Weeks, M., Fuller, M., & Herrero-Bervera, E., 1991. Geomagnetic reversal paths, *Nature*, **351**, 447.
- Larson, R. L. & Olson, P., 1991. Mantle plumes control magnetic reversal

- frequency, *Earth Planet. Sci. Lett.*, **107**, 437–447.
- Love, J. J., 1998. Paleomagnetic volcanic data and geometric regularity of reversals and excursions, *J. Geophys. Res.*, **103**, 12,435–12,452.
- Masters, T. G., Johnson, S., Laske, G., & Bolton, H. F., 1996. A shear-velocity model of the mantle, *Philos. Trans. R. Soc. London Ser. A*, **354**, 1385–1411.
- McFadden, P. L. & Merrill, R. T., 1984. Lower mantle convection and geomagnetism, *J. Geophys. Res.*, **89**, 3354–3362.
- Merrill, R. T. & McElhinny, M. W., 1996. *The Magnetic Field of the Earth*, Academic, San Diego, Calif.
- Olson, P. & Christensen, U. R., 2002. The time-averaged magnetic field in numerical dynamos with non-uniform boundary heat flow, *Geophys. J. Int.*, **151**, 809–823.
- Olson, P. & Glatzmaier, G., 1996. Magnetoconvection and thermal coupling of the Earth's core and mantle, *Philos. Trans. R. Soc. London Ser. A*, **354**, 1–12.
- Olson, P., Christensen, U., & Glatzmaier, G., 1999. Numerical modeling of the geodynamo: mechanisms of field generation and equilibration., *J. Geophys. Res.*, **104**, 10,383–10,404.
- Orszag, S. A., 1971. Numerical simulation of incompressible flows within simple boundaries. i. Galerkin (spectral) representations., *Stud. Appl. Math.*, **50**, 293–327.
- Peyret, R., 2002. *Spectral Methods for Incompressible Viscous Flow*, Springer.
- Sarson, G. R., Jones, C. A., & Longbottom, A. W., 1997. The influence of boundary region heterogeneities on the geodynamo, *Phys. Earth Planet. Int.*, **101**, 13–32.
- Simatev, R. & Busse, F. H., 2003. Patterns of convection in rotating spherical shells, *New Journal of Physics*, **5**, 97.1–97.20.

- Sreenivasan, B. & Gubbins, D., 2007. Dynamoes with weakly convecting outer layers: implications for core-boundary locking, *Geophys. Astrophys. Fluid Dyn.*, **under review**.
- Sreenivasan, B. & Jones, C. A., 2006. The role of inertia in the evolution of spherical dynamos, *Geophys. J. Int.*, **164**, 467–476.
- Tilgner, A., 1999. Spectral methods for the simulation of incompressible flows in spherical shells, *Int. J. Numer. Meth. Fluids*, **30**, 713–724.
- Vogt, P. R., 1975. Changes in geomagnetic reversal frequency at times of tectonic change: evidence for coupling between core and upper mantle processes, *Earth Planet. Sci. Lett.*, **25**, 313–321.
- Zhang, K. & Gubbins, D., 1992. On convection in the Earth's core driven by lateral temperature variations in the lower mantle, *Geophys. J. Int.*, **108**, 247–255.
- Zhang, K. & Gubbins, D., 1993. Nonlinear aspects of core-mantle interaction, *Geophys. Res. Lett.*, **20**, 2969–2972.
- Zhang, K. & Gubbins, D., 1993. Convection in a rotating spherical fluid shell with an inhomogeneous temperature boundary condition at infinite Prandtl number, *J. Fluid Mech.*, **250**, 209–232.
- Zhang, K. & Gubbins, D., 1996. Convection in a rotating spherical fluid shell with an inhomogeneous temperature boundary condition at finite Prandtl number, *Phys. Fluids*, **8**, 1141–1148.
- Zhang, K. & Gubbins, D., 2000. Is the geodynamo process intrinsically unstable?, *Geophys. J. Int.*, **140**, F1–F4.

E	RE	R/R_c	Pr	q	ϵ	R_m	Λ	comment
<i>Tomographic BC</i>								
1.2×10^{-4}	35	1.5	1	10	0.3	110	2.8	drifting dynamo
1.2×10^{-4}	35	1.5	1	10	0.6	125	2.0	almost locked, migrating equatorial patches
1.2×10^{-4}	35	1.5	1	10	0.9	140	1.4	locked dynamo
<i>$Y_2^2 BC$</i>								
1×10^{-4}	35	1.43	1	10	1	181	1.19	locked dynamo
1×10^{-4}	35	1.43	1	10	> 1.5	—	—	strong thermal winds, dynamo fails
1×10^{-4}	35	1.43	1	10	0.6	—	—	reduced boundary driven flow, fails
5×10^{-5}	30	1.13	1	15	1	233	3.80	locked dynamo
5×10^{-5}	30	0.84	2	15	1	231	4.04	almost same as $Pr = 1$
5×10^{-5}	30	1.18	0.67	15	1	—	—	increased inertia, dynamo fails

Table 1

Summary of the dynamos with laterally varying boundary heat flux considered in this study.

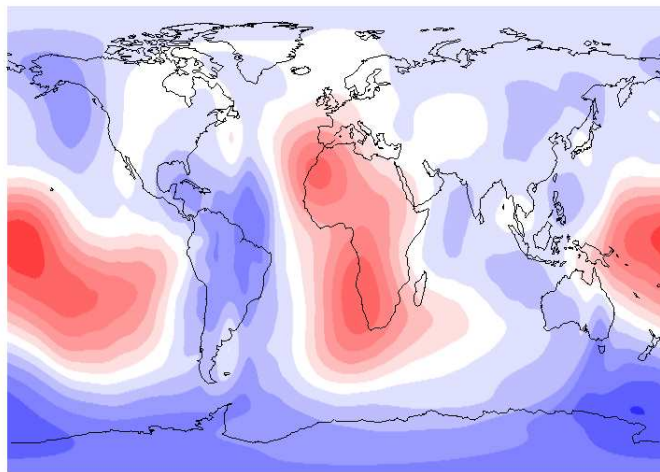


Fig. 1. Tomographic boundary condition, Masters et al. (1996). Seismic shear wave at the base of the mantle is used as a proxy for temperature in the mantle boundary layer. Cold patches occurring at the longitudes of the Atlantic and India may induce downwellings, whereas under Africa and the Pacific hot patches may suppress convection.

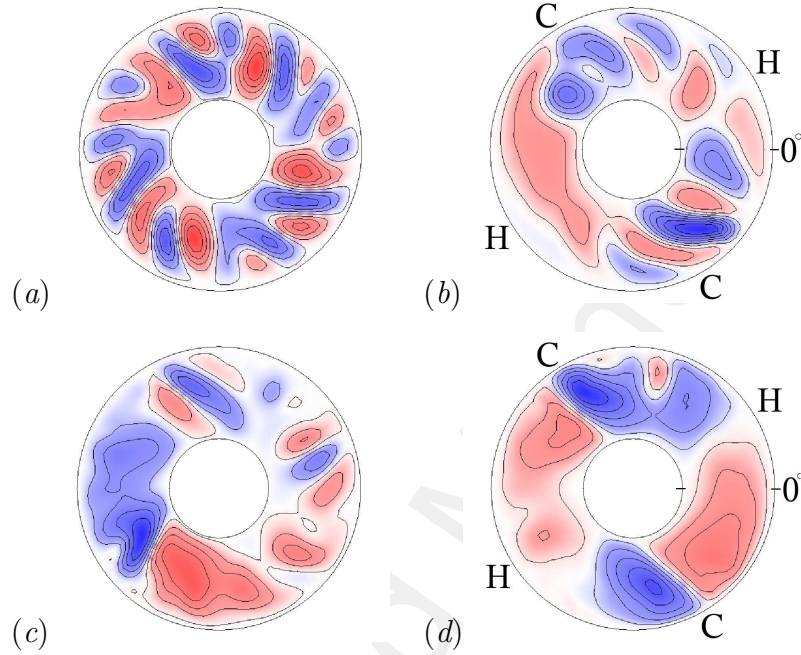


Fig. 2. Contour plots of the velocity streamfunction on the equatorial plane for solutions with $E = 1.2 \times 10^{-4}$, $q = 10$, $R = 1.5R_c$, $Pr = 1$. Cases (a) & (b) are for nonmagnetic convection, and (c) & (d) are dynamos. The figures in the left panels are for homogeneous boundary heat flux and those in the right panels correspond to inhomogeneous boundary heat flux with $\epsilon = 0.9$. The relatively cold regions at approximately 70° W and 120° E correspond to the Americas and eastern Asia respectively. The hot regions at 30° E and 150° W correspond to Africa and the Pacific. Zero longitude is marked in (b) & (d) and all angles are measured anticlockwise. The letters C and H represent cold and hot mantle respectively.

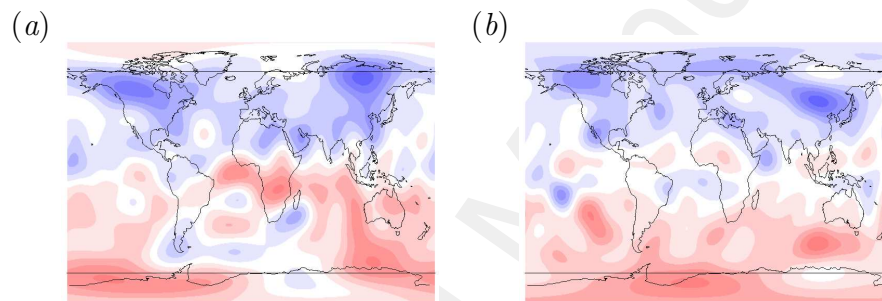


Fig. 3. The observed field in 1990 (a), B_r at the CMB and the model field (b) for $\epsilon = 0.6$; other parameters are as in Figure 2. In the model plot B_r is truncated at $l = 14$ for comparison with the observed field. In both plots western high-latitude patches have drifted slightly from the longitude of the cold boundary region. Several drifting patches of flux occur near the equator. In the model the northwestern patch has split in two (over Alaska and California).

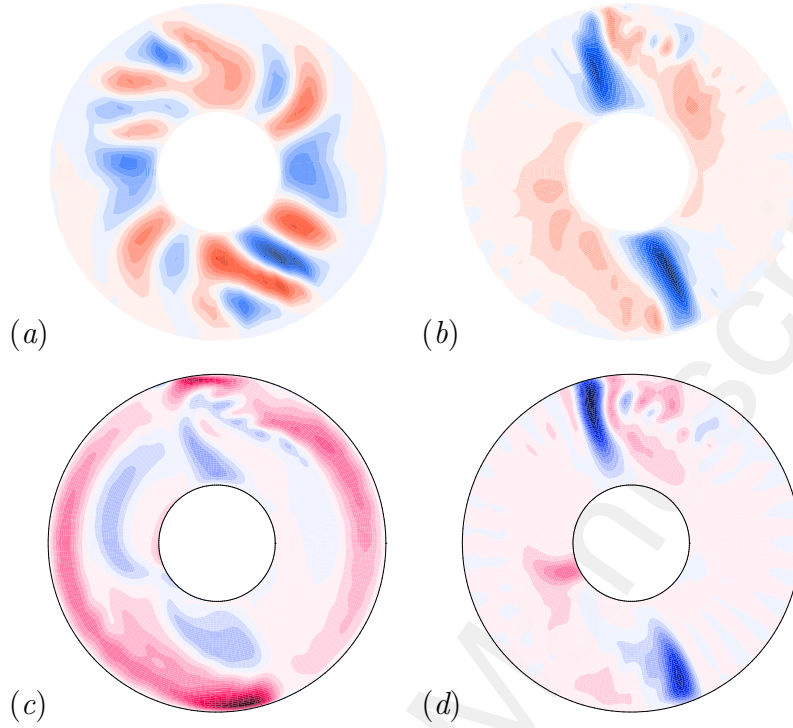


Fig. 4. (a) & (b): Equatorial section plots of the radial velocity for $\epsilon = 0.6$ (left) and $\epsilon = 1.0$ (right). (c) & (d): Horizontal section plots, at a small elevation $z = 0.1$ above the equatorial plane, of the toroidal magnetic field B_ϕ and radial field B_r , for the Y_2^2 boundary condition and $\epsilon = 1.0$. The other parameters are $E = 1 \times 10^{-4}$, $R/R_c = 1.43$, $Pr = 1$ and $q = 10$.

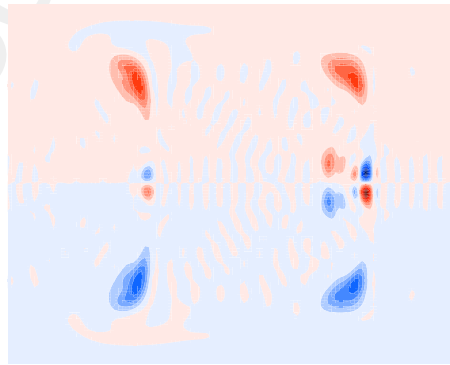


Fig. 5. Radial magnetic field at the outer boundary for the same case as Figure 4.